Agricultural and Forest Meteorology 218–219 (2016) 122–134

Contents lists available at ScienceDirect

Agricultural and Forest Meteorology

journal homepage: www.elsevier.com/locate/agrformet

Hyperspectral narrowband and multispectral broadband indices for remote sensing of crop evapotranspiration and its components (transpiration and soil evaporation)

Michael Marshall [a,b,*], Prasad Thenkabail [b], Trent Biggs [c], Kirk Post [d]

[a] Climate Research Unit, World Agroforestry Centre, United Nations Ave, Gigiri, P.O. Box 30677-00100, Nairobi, Kenya
[b] Southwestern Geographic Center, United States Geological Survey, 2255 N. Gemini Dr, Flagstaff, AZ, USA
[c] Department of Geography, San Diego State University, Storm Hall 308C, San Diego, CA, USA
[d] CSU Monterey Bay and NASA-ARC Cooperative, Chapman Science Center, 100 Campus Center, Seaside, CA 93955, USA

ARTICLE INFO

Article history:
Received 17 April 2015
Received in revised form 8 October 2015
Accepted 7 December 2015

Keywords:
Spectroscopy
Micrometeorology
Latent heat
Energy balance
HyspIRI

ABSTRACT

Evapotranspiration (ET) is an important component of micro- and macro-scale climatic processes. In agriculture, estimates of ET are frequently used to monitor droughts, schedule irrigation, and assess crop water productivity over large areas. Currently, in situ measurements of ET are difficult to scale up for regional applications, so remote sensing technology has been increasingly used to estimate crop ET. Ratio-based vegetation indices retrieved from optical remote sensing, like the Normalized Difference Vegetation Index (NDVI), Soil Adjusted Vegetation Index, and Enhanced Vegetation Index are critical components of these models, particularly for the partitioning of ET into transpiration and soil evaporation. These indices have their limitations, however, and can induce large model bias and error. In this study, micrometeorological and spectroradiometric data collected over two growing seasons in cotton, maize, and rice fields in the Central Valley of California were used to identify spectral wavelengths from 428 to 2295 nm that produced the highest correlation to and lowest error with ET, transpiration, and soil evaporation. The analysis was performed with hyperspectral narrowbands (HNBs) at 10 nm intervals and multispectral broadbands (MSBBs) commonly retrieved by Earth observation platforms. The study revealed that (1) HNB indices consistently explained more variability in ET ($\Delta R^2 = 0.12$), transpiration ($\Delta R^2 = 0.17$), and soil evaporation ($\Delta R^2 = 0.14$) than MSBB indices; (2) the relationship between transpiration using the ratio-based index most commonly used for ET modeling, NDVI, was strong ($R^2 = 0.51$), but the hyperspectral equivalent was superior ($R^2 = 0.68$); and (3) soil evaporation was not estimated well using ratio-based indices from the literature (highest $R^2 = 0.37$), but could be after further evaluation, using ratio-based indices centered on 743 and 953 nm ($R^2 = 0.72$) or 428 and 1518 nm ($R^2 = 0.69$).

1. Introduction

Evapotranspiration (ET) is the process by which mass/energy is exchanged between the surface and atmosphere via evaporating moisture from soil, open water, and wet plant canopies or transpiring moisture from photosynthesizing canopies (Chapin et al., 2011). It is therefore a critical component of several physical and biological processes at the cellular, leaf, plant, canopy, and landscape scale (Katul et al., 2012). In most regions of the world, water loss (the ratio of ET to precipitation) is increasing in response to global warming (Huntington, 2006). This has particularly strong implications for irrigated agriculture, which currently accounts for 70% of the world's surface water and groundwater withdrawals and whose demand is expected to increase by 22% in 2050 (Rosegrant et al., 2009). The increase in demand from irrigated agriculture combined with increasing demand from other competing and expanding sectors, means that better agricultural water management is necessary. Effective water management includes improved monitoring, assessment, and forecasting of crop ET, in order to develop and evaluate water-saving strategies (Evans and Sadler, 2008). In situ estimates of crop ET are difficult to extrapolate to scales for regional processes and applications (Jung et al., 2009), so Earth observation remote sensing-based ET models calibrated/validated with in situ data are increasingly used (Dam et al., 2006). These models, however, have bias and error, particularly with regards to the

* Corresponding author at: Climate Research Unit, World Agroforestry Centre, United Nations Ave, Gigiri, P.O. Box 30677-00100, Nairobi, Kenya.
E-mail addresses: m.marshall@cgiar.org (M. Marshall), pthenkabail@usgs.gov (P. Thenkabail), tbiggs@mail.sdsu.edu (T. Biggs), kpost@csumb.edu (K. Post).

http://dx.doi.org/10.1016/j.agrformet.2015.12.025

partitioning of ET into its components (transpiration and soil evaporation) (Gowda et al., 2008).

Evapotranspiration modeling approaches involving Earth observation remote sensing data are reviewed in Biggs et al. (2015), Courault et al. (2005), Diak et al. (2004), Glenn et al. (2007), Kalma et al. (2008), Kustas and Norman (1996), and Wang and Dickinson (2012). These models can be categorized as vegetation-based, temperature/energy balance, and scatterplot approaches. Vegetation-based methods estimate ET or its energy equivalent (LE: latent heat) as a function of ratio-based vegetation indices derived from optical Earth observation, the atmospheric demand for water vapor (PET: Potential Evapotranspiration) or vegetation specific analog (crop reference ET: Allen et al., 1998), and temperature/moisture constraints. PET is estimated using either the Penman–Monteith (Leuning et al., 2008; Mu et al., 2011, 2007; Nishida et al., 2003) or Priestley–Taylor (Fisher et al., 2008) equations. Temperature/energy balance approaches estimate temperature from thermal infrared remote sensing, which is either used to estimate LE directly (Simplified Surface Energy Balance: Senay et al., 2007) or indirectly as a residual of the energy balance equation. The two-source energy balance approaches (Two Source Energy Balance – Norman et al., 1995 and Atmosphere-Land Exchange Inverse – Anderson et al., 1997) use a ratio-based index to separate land surface temperature into canopy and soil heat components from which transpiration and evaporation are estimated, respectively. Scatterplot methods (Gillies et al., 1997; Moran et al., 1994) are a close relative of temperature/energy balance methods. Latent heat is bounded by vertices of a triangle or trapezoid that represent fully transpiring (high ratio-based index, "cold" temperature) or low-transpiring vegetation (low ratio-based index, "hot" temperature) over an area of interest.

Whether vegetation-based, temperature/energy balance, or scatterplot methods are used, ratio-based indices, derived from the optical range of remote sensing, play a critical role in crop ET models (Glenn et al., 2010), particularly for ET partitioning (Wang et al., 2014). The primary indices used are the Normalized Difference Vegetation Index (NDVI – Rouse, 1974) and Soil Adjusted Vegetation Index (SAVI – Huete, 1988) from which the fraction of photosynthetically active radiation intercepted by the canopy (F_{IPAR}) is computed. These indices are derived from visible red and near infrared (NIR) remote sensing reflectance representing several convolved wavelengths (i.e. MSBBs: multispectral broadbands), because plant material strongly absorbs visible red light and scatters NIR due to the spectral properties of plant chlorophyll, accessory pigments, and the alignment of cell walls (Ollinger, 2011). SAVI is used together with or in place of NDVI, because it is less sensitive to soil background and saturation in dense canopies. The Enhanced Vegetation Index (EVI) (Huete et al., 2002) has become a widely used alternative to SAVI, because it incorporates a blue reflectance broadband, which reduces atmospheric effects that impact NDVI and SAVI. The Normalized Difference Water Index (NDWI) and Global Vegetation Moisture Index exploit leaf water absorption in the Shortwave Infrared (SWIR) and are the most commonly used non-red-NIR indices for ET estimation (Guerschman et al., 2009; Lu and Zhuang, 2010).

Hyperspectral remote sensing, unlike MSBB remote sensing, involves hundreds of spectral narrowbands that are sensitive to distinct biophysical and biochemical characteristics, and facilitate atmospheric correction and the unmixing of heterogeneous surfaces with "idealized" spectra (Goetz, 2009). Although hyperspectral remote sensing has been used for agricultural modeling applications that require direct or relative estimates of light-absorbing plant pigments, plant water content, or dry plant residues (Ustin et al., 2004), its application in ET modeling is relatively unstudied (see Rodriguez et al., 2011 for a review of relevant opportunities).

There is a general lack of studies that utilize MSBB ratio-based vegetation indices (MSVIs) other than NDVI, SAVI, EVI, NDWI, and more importantly, HNB ratio-based vegetation indices (HVIs) in crop ET models. This paper employs empirical methods and in situ spectroradiometric and eddy covariance/surface renewal data to (1) identify potentially useful MSVIs and HVIs over the entire optical range for estimation of crop ET and its components (transpiration and evaporation) and (2) compare these indices with existing MSVIs and HVIs from the literature to inform the ET modeling community, and more importantly, upcoming global mapping imaging spectroradiometric missions, such as the Hyperspectral Infrared Imager (http://hyspiri.jpl.nasa.gov/).

2. Methods

2.1. Study area

In 2011 and 2012, field campaigns were conducted to estimate ET using field and remote sensing methods in the Central Valley of California – an important agro-ecosystem of the United States (CDFA, 2013). Spectroradiometric and ancillary biophysical data, including crop height, leaf area index, and F_{IPAR} were collected in the fetch of seven micrometeorological stations during three visits in the summer growing season coinciding with the sprouting (May–June), flowering/tasseling (June–July), and senescence (July–August) stages of crop growth (Fig. 1 and Table 1). For two of the stations (Davis and on Twitchell Island), spectroradiometric and ancillary biophysical data were collected for both 2011 and 2012, because they were operational for multiple growing seasons. The other stations only operated over one growing season. Spectroradiometric and ancillary biophysical data were collected on the same day of each visit. Micrometeorological stations recorded weather and energy balance data at regular intervals throughout the growing season.

The fetch consisted of soil, water, and vegetation, which conditioned air parcels recorded as the turbulent energy flux by the station (Schuepp et al., 1990). The fetch extent was defined by the dominant daytime summer wind direction and generally spanned the length of the field adjacent to each station (<450 m). Each station was located in large, flat, irrigated, and homogenous fields. The fields under measurement consisted of three widely cultivated and water-intensive field crops in California: cotton, maize, and rice. Each field represented diverse soil types and climatology of the Central Valley.

2.2. Spectroradiometric data and processing

Field spectra were collected using an Analytical Spectral Devices (ASD) portable spectroradiometer (Field Spec Pro 3: www.asdi.com). The Field Spec Pro 3 detects light scattered by a canopy over the optical range (350–2500 nm) at 1–10 nm intervals depending on the spectral position. Light is captured with a fiber optic cable and was constrained in this study by an 18° field of view (FOV) fore-optic. The fore-optic was mounted to a pole pointed at nadir and at a fixed height (1.5 m for cotton and rice and 2.5 m for maize) ±2 h solar noon to minimize inconsistencies due to canopy shadow and sun angle. The FOV corresponded to 1 m^2 quadrats over which ancillary biophysical data was measured on the same day. Spectra were collected for ten evenly spaced quadrats in the footprint of each micrometeorological station. Approximately five replicates were collected at random locations in the quadrat. A replicate spectrum consisted of Field Spec Pro internally averaged spectra (30 for optimal environmental conditions and 40 for sub-optimal environmental conditions).

Table 1
Summary table of the micrometeorological stations (SR = surface renewal and EC = eddy covariance) used in the experiment. Each station had an official identifier (ID) for the analysis. *N* is the length of the time series in days over which weather and energy flux data was recorded, T_A is the long-term (1971–2000) average daily air temperature for June–August (°C), and PPT is the long-term (1971–2000) annual cumulative precipitation (mm). Dominant soil type (Soil), elevation (Elev) in meters, and climatological means were extracted from the Soil Survey Geographic Database (www.nrcs.usda.gov), the National Elevation Dataset (http://ned.usgs.gov/), and the Parameter-Elevation Regressions on Independent Slopes Model downscaled to 270 m resolution (Daly et al., 1994; Thorne et al., 2012), respectively.

Station	ID	Latitude	Longitude	Crop type	Method	Year	Elev	Soil	*N*	T_A	PPT	Source
Davis	*MADAV01*	38.65	−121.81	Maize	SR	2011	22	Alfisols	100	34.0	531	CADWR
Twitchell Island	*RITWI10*	38.11	−121.65	Rice	EC	2011	−1	Histosols	118	31.3	429	UC Berkeley
Biggs	*RIBIG01*	39.45	−121.71	Rice	SR	2011	31	Entisols	92	33.7	610	UC Davis
Wilson	*RIWIL01*	39.17	−122.10	Rice	SR	2012	18	Vertisols	106	33.6	434	UC Davis
Staten Island (Wet)	*MASTA01*	38.18	−121.51	Maize	SR	2012	−2	Mollisols	122	31.8	440	USGS
Staten Island (Dry)	*MASTA02*	38.17	−121.51	Maize	SR	2012	−2	Histosols	122	31.8	437	USGS
Five Points	*COFIV01*	36.35	−120.11	Cotton	SR	2012	84	Aridisols	122	34.8	191	NASA
Davis	*MADAV10*					2012			86			
Twitchell Island	*RITWI09*					2012			122			

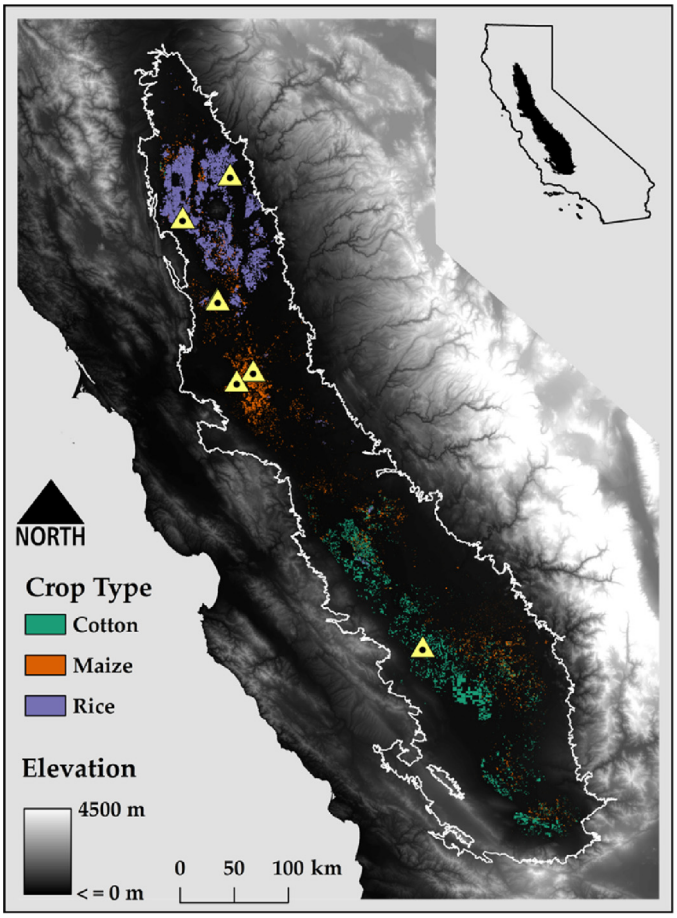

Fig. 1. The Central Valley of California. Energy balance data from seven micrometeorological towers and hyperspectral narrowband data from a portable spectroradiometer were collected for 2011 and 2012 for three important water-intensive field crops: cotton, maize, and rice (•). The study sites are overlaid with elevation and crop layers extracted from the National Elevation Dataset (http://ned.usgs.gov/) and National Agricultural Statistics Service Cropland Data Layer for 2012 (http://nassgeodata.gmu.edu/CropScape/), respectively.

The Field Spec Pro 3 includes software (ViewSpec Pro®) that converts the raw digital numbers into radiance (W sr^{-1} m^{-2}). Radiance was standardized (i.e. converted to reflectance 0–100%) in ViewSpec Pro with calibration spectra retrieved from a reference or "white" panel. The white panel represents present sky conditions. Since these conditions vary considerably throughout the day, white reflectance was captured every 2–10 min, with frequency increasing as cloud cover increased. In the majority of cases, however, cloud cover was very low.

Table 2
Moderate Resolution Imaging Spectroradiometer bands to which hyperspectral narrowbands were averaged.

Band #	Spectral range (nm)	Spectral color
Band 1	620–670	Red
Band 2	841–876	Very Near Infrared
Band 3	459–479	Blue
Band 4	545–565	Green
Band 5	1230–1250	Near Infrared
Band 6	1628–1652	Shortwave Infrared-1
Band 7	2105–2155	Shortwave Infrared-2

The replicates underwent additional preprocessing before the analysis. Strong absorption/scatter bands not related to the canopy exist in field spectra, due to the characteristics of various compounds in the atmosphere. These bands were omitted and include 350–390 nm (O_3), 1350–1450 nm (H_2O and CO_2), 1790–2000 nm (H_2O and CO_2), and 2300–2500 nm (H_2O and CO_2). In order to reduce redundancy in adjacent wavelengths that typically represent similar spectral information (see Thenkabail et al., 2000); the spectra were integrated or convolved to 10 nm intervals. The convolution yielded 157 unique hyperspectral narrowbands (HNBs) from 428 to 2295 nm after omitting contaminated bands. Further details on these steps can be found in Marshall and Thenkabail (2015). The replicates were then averaged, so that each quadrat had one spectrum and then all quadrats in the footprint of a given station were averaged, so that each station had an areal average for each visit. These steps aided in interpretation of the micrometeorological data, by significantly reducing noise caused by the subtle changes in weather and spectral properties within the fetch.

In order to compare the performance of HVIs and MSVIs, the spectra were convolved to Moderate-Resolution Imaging Spectroradiometer (MODIS) spectral bands (Table 2) using the ViewSpec Pro package. MODIS Terra (launched in 1999) and its companion MODIS Aqua (launched in 2002) provide global coverage of several MSSBs every 1–2 days and are widely used to understand regional processes (García-Mora et al., 2012). MODIS data were not used directly for the analysis, because of scale differences between field spectra and the MODIS sensor.

For the remainder of this paper, spectral ranges are identified by their colors: visible blue (450–495 nm), visible green (495–570 nm), visible red (620–680 nm), NIR (730–1000 nm), Shortwave Infrared-1 (SWIR1: 1000–1700 nm), and Shortwave Infrared-2 (1700–2500 nm). The "red-edge" refers to the region where the rapid transition between chlorophyll absorption in the visible red to scatter in the NIR occurs (680–730 nm). MODIS retrieves spectral data in the optical range (visible, NIR, SWIR1, and

SWIR2) consisting of seven channels at 250–500 m spatial resolution (Huete et al., 2002).

2.3. Other biophysical data

For each quadrat, crop height, F_{IPAR}, and LAI were also measured. Like the field spectra, areal averages were used for the analysis. Crop height (cm) was determined with measuring tape (cotton and rice) or a telescoping measuring pole (maize) at 3–5 random locations in each quadrat and averaged. F_{IPAR} and LAI were recorded with a Decagon Devices, Inc. AccuPAR LP-80® (http://www.decagon.com/). The LP-80 is a ceptometer that records above canopy and below canopy incoming shortwave radiation (SW). The LP-80 consists of a data logger and probe that contains 80 photosensors at 1 cm spacing (Decagon, 2010). The probe was placed under the canopy to record incoming below canopy SW, while a small external sensor connected to the data logger and mounted on a pole above the canopy, recorded incoming above canopy SW simultaneously. Five replicates, each of which represented 10 LP-80 internally averaged estimates, were taken at random locations below the canopy. Like the spectroradiometric data, the ceptometer data was recorded ±2 h solar noon to reduce solar illumination effects. The LP-80 records SW in units of $\mu mol\ m^{-2}\ s^{-1}$. The ratio of below canopy SW to above canopy SW equals F_{IPAR}. Solar zenith angle and fractional beam readings are computed by the LP-80 internally, leaving only one remaining user-defined input (canopy clumping parameter). The canopy clumping parameter was computed just prior to daily ceptometer readings. The clumping parameter was estimated as the ratio of the vertical gap fraction to the horizontal gap fraction, which was determined by the shadows cast on a 1 m^2 gridded screen placed perpendicularly to and underneath the canopy, respectively.

2.4. Micrometeorological data and processing

The micrometeorological stations collected data on weather (minimum/maximum daily air temperature, wind speed and direction, and dewpoint temperature) and energy flux (net radiation – R_N, sensible heat – H, latent heat – LE, and soil heat flux – G). LE was provided in units of $W\ m^{-2}$ and recorded at 30-min intervals. With the exception of Twitchell Island, there were no data gaps in the LE data and it was converted to ET ($MJ\ m^{-2}\ d^{-1}$) by multiplying the daily average by the number of hours in a day. For Twitchell Island, days with greater than three 30-min gaps in a day were assigned as missing for the entire day. LE was computed using either the surface renewal (SR) or eddy covariance (EC) approach. With surface renewal (SR), fine-wire thermocouples at the surface (above the canopy) are used to detect "ramping events" representing sensible heat flux scalar flux densities (Paw U et al., 1995). A ramp event occurs when an air parcel just above the surface is swept away after an energy exchange with the surface and replaced by an air parcel directly above it. These ramps are measured in terms of temperature and combined with structure functions to estimate H. LE is then computed as a residual of R_N, G, and H. In the eddy covariance (EC) approach, flux is determined from the movement of eddies over large and homogenous footprints (Baldocchi et al., 1988). LE is measured as the change in water vapor concentration as one eddy lifts, while another eddy sinks. Unlike SR, which measures exchange at a single point, EC assumes that the exchange of air parcels covaries with vertical wind shear over the fetch, necessitating the use of the turbulent flow formula and Reynold's decomposition for simplification. Vertical wind shear is measured with a sonic anemometer, while water vapor concentration is measured at the surface and at height with hygrometers.

In the EC approach, LE and H are measured independently, so an imbalance on the order of 20% is not uncommon (Wilson et al., 2002). To account for this lack of closure, the LE closure method (Falge et al., 2005) was applied, where LE is computed as a residual of R_N, G, and H. The LE closure method, therefore, assumes that all of the error is in the LE term. The LE closure method was selected, because there is no consensus on which closure approach to use (Foken, 2008) and it is consistent with SR. The majority of the sites used the SR approach. For the only two stations in this study that employed both EC and SR techniques (Biggs and Wilson), there was a high level of agreement between the two methods on a daily time step: R^2 (coefficient of determination) = 0.96–0.97 (Fig. 2). For this reason, the SR approach was chosen where available. The one exception was Twitchell Island, because SR was not used there. Details of the Twitchell Island tower can be found in Hatala et al. (2012).

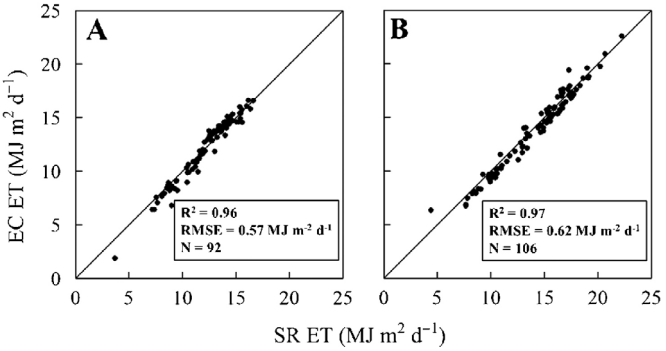

Fig. 2. Scatterplots of evapotranspiration (ET) measured with the eddy covariance method (EC) versus ET measured with the surface renewal method (SR) for two micrometeorological towers in rice fields that employed both EC and SR methods over the growing season: (a) Biggs and (b) Wilson. The lines represent a 1:1 relationship through the origin (0, 0). R^2 = coefficient of determination, RMSE = root mean squared error, and N = number of samples.

Evapotranspiration was partitioned into transpiration (ET_C) and soil evaporation (ET_S) using a remote sensing approach to partitioning ET (Blyth and Harding, 2011), which assumes that transpiration is driven primarily by the fraction of incoming radiation that is absorbed by the canopy for photosynthesis (F_{APAR}) (Brunsell and Anderson, 2011). Assuming that the evaporation of precipitation that is intercepted by the canopy is zero, soil evaporation can be solved as a residual of evapotranspiration and transpiration ($ET_S = (1 - F_{APAR}) \cdot ET$). This assumption is reasonable, because the evaporation of water that is intercepted by the canopy is only significant in humid forests where rainfall and woody biomass are abundant (Kang et al., 2012), the condition of which does not exist for irrigated field crops in the Central Valley during the primary growing season. We selected this method over field methods used for partitioning ET (see Kool et al., 2014 for a recent review), because (1) our aim was to identify vegetation indices that improve remote sensing ET models and (2) current field methods are complicated and expensive, with varying degrees of accuracy. The third assumption made in the partitioning approach taken was that F_{APAR} is approximately equal to F_{IPAR} measured with the ceptometer. This assumption is also reasonable, since field crop canopies typically absorb 80–90% of the intercepted radiation for photosynthesis (Monteith, 1969).

For the analysis, 10-day average ET (prior and including the day of each visit) was used instead of ET on the day of each visit. This was done, because vegetation indices represent time-averaged environmental conditions and plants take several days, weeks, or longer to acclimate (i.e. reorganize pigments, membranes, and enzymes) to new extraneous conditions (Pearcy and Sims, 1994). The summer growing season in the Central Valley is largely cloud-free, so the averages were taken over the entire 10-day period for each visit. Since one of the stations was not installed during the first visit,

Table 3
Selected subset of remote sensing based hyperspectral narrowband and multispectral broadband ratio based indices selected from the literature for evapotranspiration simulation. Multispectral broadbands (% reflectance) are identified by their Moderate-Resolution Imaging Spectroradiometer (MD) band number, while HNBs (% reflectance) are identified with "λ" and the spectroradiometer wavelength centroid used in this study. Each index has been used in the past for specific canopy properties: "structure" in this case refers to properties such as biomass, leaf area index, or fraction of photosynthetically active radiation; "water" refers to leaf water content; and "physiology" refers to properties related to stress such as light-use efficiency or red-edge.

	Abbreviation	Formula	Purpose	Source
Mutispectral broadband indices				
Simple ratio	Simp	$\frac{MD02}{MD01}$	Structure	Pearson and Miller (1972)
Normalized Difference Vegetation Index	NDVI	$\frac{MD02-MD01}{MD02+MD01}$	Structure	Rouse (1974)
Enhanced Vegetation Index	EVI	$\frac{2.5*(MD02-MD01)}{MD02+6*MD01-7.5*MD03+1}$	Structure	Huete et al. (2002)
Visible Atmospherically Resistant Index	VARI	$\frac{MD04-MD01}{MD04+MD01-MD03}$	Structure	Gitelson et al. (2002)
Normalized Difference Water Index (1)	NDWI1	$\frac{MD02-MD05}{MD02+MD05}$	Water	Gao (1996)
Normalized Difference Water Index (2)	NDWI2	$\frac{MD02-MD06}{MD02+MD06}$	Water	Chen et al. (2005)
Normalized Difference Water Index (3)	NDWI3	$\frac{MD02-MD07}{MD02+MD07}$	Water	Chen et al. (2005)
Hyperspectral Narrowband Indices				
Hyperspectral Vegetation Index	HVI	$\frac{\lambda 743}{\lambda 692}$	Structure	Gitelson et al. (1996)
Hypersepctral Normalized Difference Vegetation Index	HNDVI	$\frac{\lambda 814-\lambda 672}{\lambda 814+\lambda 672}$	Structure	Oppelt and Mauser (2004)
Greenness Index	GI	$\frac{\lambda 539}{\lambda 682}$	Structure	Zarco-Tejada et al. (2005)
Hyperspectral Normalized Difference Water Index	HNDWI	$\frac{\lambda 845-\lambda 1256}{\lambda 845-\lambda 1256}$	Water	Gao (1996)
Normalized Difference Infrared Index	NDII	$\frac{\lambda 845-\lambda 1649}{\lambda 845-\lambda 1649}$	Water	Hardisky et al. (1983)
Water Index	WI	$\frac{\lambda 895}{\lambda 983}$	Water	Penuelas et al. (1997)
Photochemical Reflectance Index	PRI	$\frac{\lambda 529-\lambda 580}{\lambda 529-\lambda 580}$	Physiology	Gamon et al. (1992)
Red-Edge Vegetation Stress Index	RVSI	$0.5(\lambda 722+\lambda 763)-\lambda 733$	Physiology	Merton and Huntington (1999)
Modified Chlorophyll Absorption Ratio Index	MCARI	$\frac{\lambda 712[(\lambda 712-\lambda 682)-0.2(\lambda 712-\lambda 539)]}{\lambda 682}$	Physiology	Daughtry et al. (2000)

the final sample size for the analysis was 26 (9 10-day averages × 3 visits − 1) micrometeorological–spectroradiometric sample pairs.

2.5. Vegetation indices and evaluation

Spectral data were evaluated in an exploratory manner across the full range of HVIs and MSVIs available for this study, which may or may not have been identified previously in the literature, and then compared to HVIs and MSVIs identified from the literature. The ratio-based vegetation index approach was selected, because (1) it is the most common method used to integrate spectral information in the optical range into ET models and (2) the sample size for the analysis was small ($N = 26$), which could lead to over-fitting with other data mining techniques. The relationship between ET and the vegetation indices were assumed linear, because linear transformations (exponential, quadratic, reciprocal, and logarithmic) added little explanatory power ($\Delta R^2 < 0.04$). First and second derivative transformations are sometimes performed on spectra, because they enhance the vegetation signal and minimize the effects of soil or other background spectra (Thorp et al., 2004). These transformations provided little additional explanatory power as well.

The exploratory phase of the analysis was performed by deriving every possible HNB or MSBB two-band combination and comparing them to ET, ET_C, and ET_S for all three crops:

$$\frac{R_2 - R_1}{R_1 + R_2} \quad (1)$$

where R_1 is reflectance for a given HNB or MSBB and R_2 is reflectance for another given HNB or MSBB. Since several thousand HVIs were involved, lambda–lambda contour plots (Thenkabail et al., 2000) were used to pinpoint the most highly correlated two-band combinations, while histograms were used to show the frequency with which each band produced an R^2 in the top 75th percentile of all R^2 values. The analysis was performed using all the crops and not on a per-crop basis, because (1) the sample size was small and (2) the purpose of the analysis was to show the universality of the relationships. The vegetation indices that produced the highest R^2 and lowest root mean squared error (RMSE) for ET, ET_C, and ET_S were plotted and compared with vegetation indices from the literature.

The HVIs and MSVIs commonly used in the literature and selected for the analysis, along with their primary function and literary source, are shown in Table 3. In all, 16 indices were selected. Many of the indices were taken from three studies that analyzed the sensitivity of several ratio-based indices to crop biomass (Gnyp et al., 2014), nitrogen availability/water stress (Perry and Roberts, 2008), and species distribution (Thenkabail et al., 2013). Simple ratio (Simp) and NDVI are widely used with the AVHRR MSBB sensor. EVI and VARI are common alternatives to Simp and NDVI and used extensively with the MODIS and Landsat MSBB sensors. These indices are especially sensitive to canopy structure (e.g. biomass, LAI, F_{APAR}), so here we refer to them as "structure-based." NDWIs are also regularly employed by Landsat and MODIS sensors to monitor water stress, because they involve NIR and SWIR channels, which are sensitive to leaf water content (Chandrasekar et al., 2010), so here we refer to them as "water-based." Several equivalent indices, such as the Hyperspectral Normalized Difference Vegetation or Water Index, have been developed with HNBs to estimate canopy structure and water properties as well. Other indices, which are sensitive to plant physiology, stress, and non-water biochemistry, however, are unique to the hyperspectral domain. These include the Photochemical Reflectance Index (PRI), Red-Edge Vegetation Stress Index (RVSI), and Modified Chlorophyll Absorption Ratio Index (MCARI), which are sensitive to light-use efficiency, red-edge, and leaf pigments. As above, vegetation indices from the literature were plotted and evaluated using R^2 and RMSE.

3. Results

3.1. Summary of non-spectral field measurements

The ancillary biophysical data is summarized in Table 4. Maize was the tallest crop (maximum $\mu = 320.45$ cm), while rice was the shortest (minimum $\mu = 52.18$ cm). The height varied considerably across the crops, with maize and rice both exhibiting the largest

Table 4
Summary table of the biophysical data collected at each micrometeorological tower or in its footprint. Crop height (Height) is measured in cm, Leaf Area Index (LAI) is in units of $m^2\ m^{-2}$, and LE is daily average latent heat measured in $MJ/m^2/d$. The fraction of intercepted photosynthetically available radiation (F_{IPAR}) is expressed as a decimal percent. Values are derived from the three measurements taken over the growing seasons ($N = 26$).

Station	ID	Height (μ)	Height (σ)	LAI (μ)	LAI (σ)	F_{IPAR} (μ)	F_{IPAR} (σ)	LE (μ)	LE (σ)
Davis	*MADAV01*	320.45	33.88	3.67	0.77	0.93	0.02	12.83	3.65
Twitchell Island	*RITWI10*	52.18	21.58	2.51	2.85	0.54	0.47	15.12	5.13
Biggs	*RIBIG01*	86.42	2.95	4.11	1.26	0.95	0.04	12.21	2.48
Wilson	*RIWIL01*	72.33	35.65	4.62	1.65	0.68	0.35	14.21	3.41
Staten Island (Wet)	*MASTA01*	305.03	3.44	5.97	1.00	0.95	0.04	7.74	2.99
Staten Island (Dry)	*MASTA02*	309.00	19.66	5.68	0.76	0.91	0.01	7.84	3.35
Five Points	*COFIV01*	67.73	34.76	3.84	2.25	0.71	0.35	13.35	3.58
Davis	*MADAV10*	286.57	12.24	6.22	2.14	0.96	0.03	10.22	8.40
Twitchell Island	*RITWI09*	53.63	28.49	2.50	2.10	0.57	0.44	14.38	3.17

($\sigma = \pm 33.88$ and 35.65 cm) and smallest ($\sigma = \pm 2.95$ and 3.44 cm) variability. LAI was highest for maize, a planophile (maximum $\mu = 6.22\ m\ m^{-2}$), and lowest for rice, an erectophile (minimum $\mu = 2.51\ m\ m^{-2}$), though no consistencies were observed between crop growth stage and LAI. F_{IPAR} increased with height for rice, but not for maize. For rice, ET tended to decrease with height during the latter part of the growing season. For maize, however, this relationship was not as obvious. Unlike rice, maize LAI decreased during senescence when the leaves wilted and dried out. In addition, maize has a longer growing season than the other crops, so measurements were taken relatively closer to one another as a fraction of the total growing season, because all of the crops were measured during the same visits. Cotton was the strongest planophile measured and has a shorter growing season than maize, so the standard deviation for F_{IPAR} was quite large ($\sigma = \pm 0.35$).

3.2. Ratio-based indices from this study

The lambda-lambda plots and histograms revealed that the most important spectral regions were the red-edge and visible blue for ET, red-edge for ET_C, and NIR for ET_S. The HVIs that correlated most closely with ET, along with the relative frequency of HNBs in the highest correlated two-band vegetation indices are shown in Fig. 3a and b. The most highly correlated HVIs with ET were in the red-edge at 672 nm and visible blue between 428 and 478 nm, with the highest centered on 672 and 448 nm ($R^2 = 0.51$). Other important regions were in the NIR (943 and 1094 nm) and SWIR1 (1175 and 1296 nm). Although the most highly correlated wavelengths were in the red-edge and visible blue, the wavelengths with the highest frequency of high R^2 values were in the NIR (794, 855, and 916 nm), meaning, unlike the red-edge and visible blue wavelengths, the NIR wavelengths correlated well with ET across a large range of wavelengths. Similar plots for ET_C and ET_S are shown in Fig. 4a–d. The correlation between ET components and HVIs tended to be much higher across a larger range of wavelengths than ET and HVIs. For ET_C, the most important HVIs, similar to ET, were centered on 672 nm. These HVIs were paired strongly with several NIR and SWIR1 wavelengths (722–1750 nm), with the highest correlated HVI centered on 672 and 733 nm ($R^2 = 0.68$). Other, but lower correlated wavelengths were seen across the visible, NIR, and SWIR1. The 75th percentile histogram revealed that 672 nm was not only the most highly correlated, but was also the

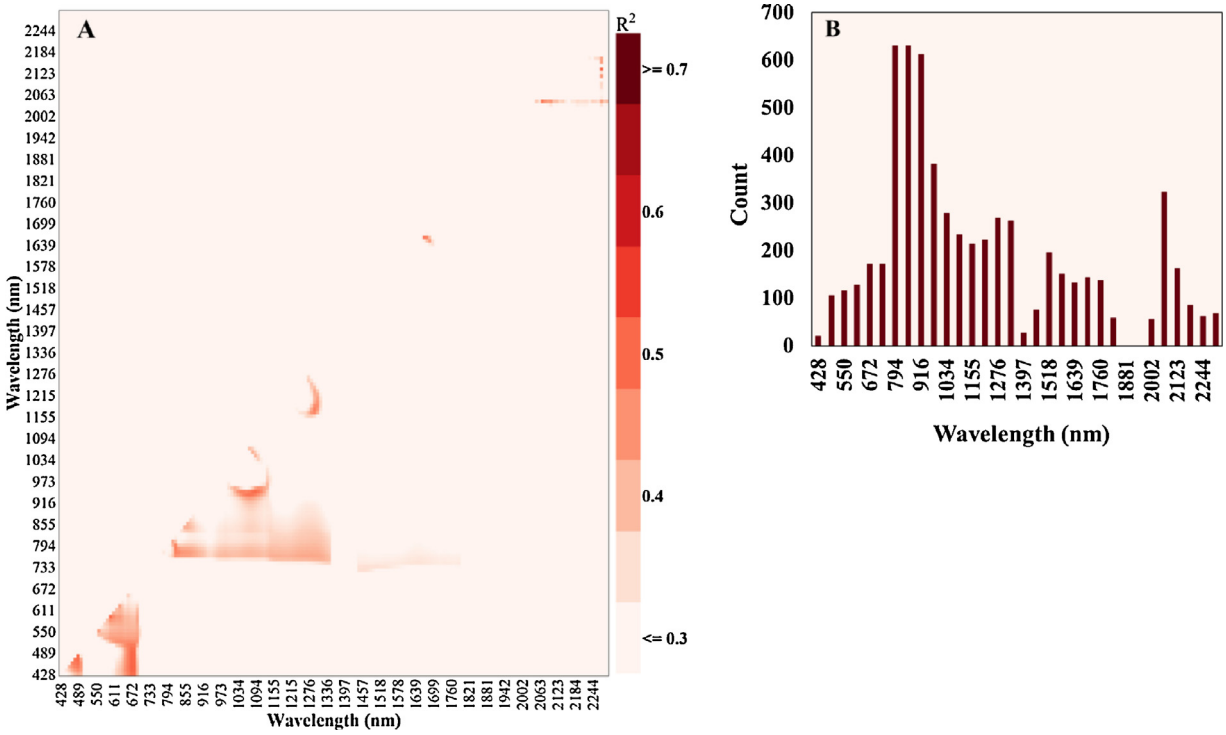

Fig. 3. (a) Lambda–lambda contour plots showing the coefficient of determination (R^2) for the regression between evapotranspiration and a given index at all the sites ($N = 26$) for every combination of two-band hyperspectral narrowbands at 10 nm intervals from 428 to 2295 nm and (b) histogram of the frequency of hyperspectral narrowbands for those bands that were in the upper 75th percentile of highest R2 values in the contour plots.

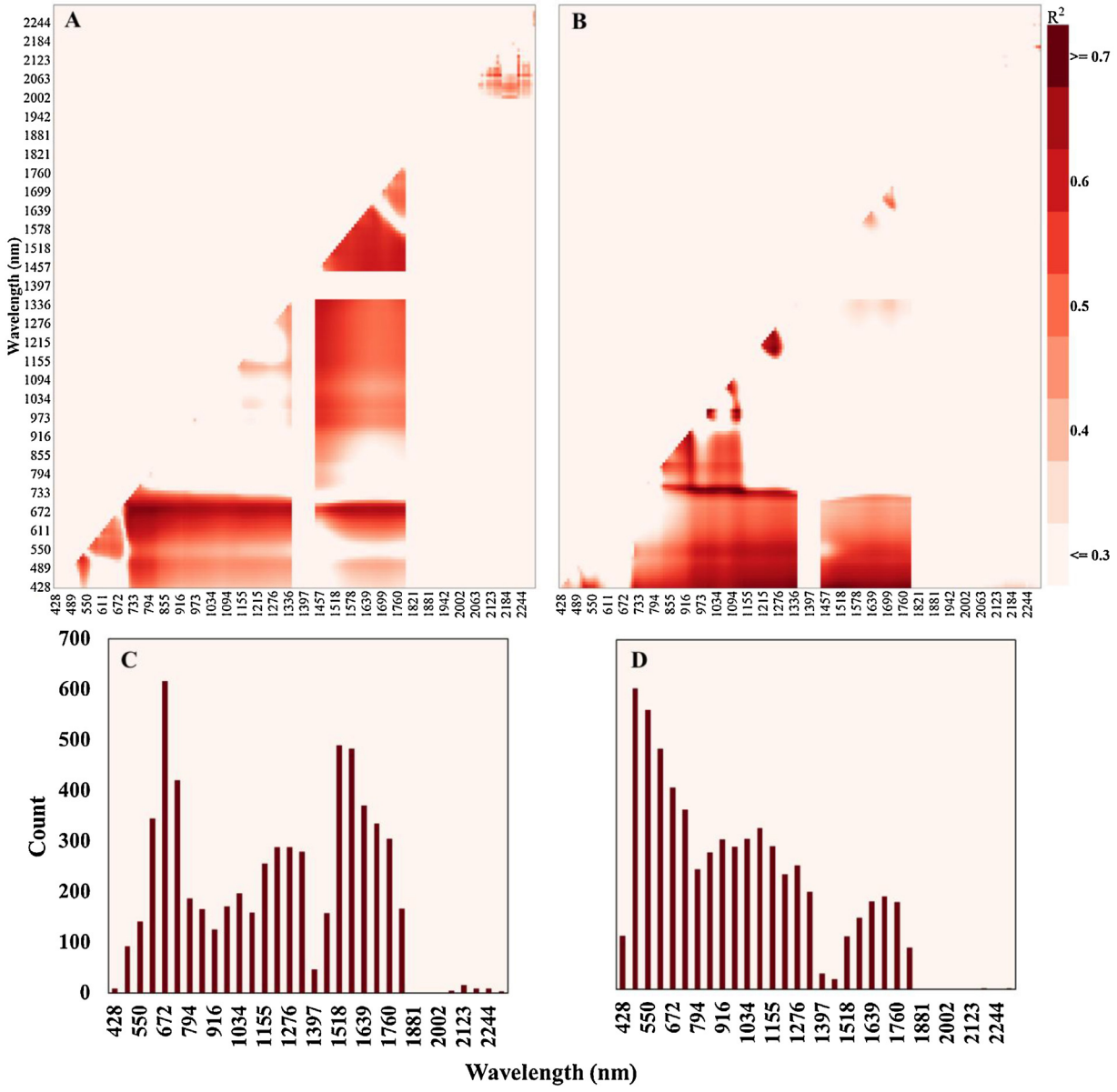

Fig. 4. Lambda–lambda contour plots showing the coefficient of determination (R^2) for every two-band hyperspectral narrowband combination at 10 nm intervals from 428 to 2295 nm for (a) transpiration and (b) soil evaporation ($N = 26$). Corresponding to these plots are histograms that show the frequency of hyperspectral narrowbands for the upper 75th percentile of highest R^2s in the contour plots for (c) transpiration and (b) soil evaporation.

wavelength with the most frequent occurrences of high R^2 as well. The correlations between HVIs and ET_S tended to be higher than for ET_C, though over a narrower range of wavelengths. The most highly correlated HVIs were centered on 743 nm across a range of NIR and SWIR1 wavelengths (916–1155 nm), with the highest HVI centered on 743 and 953 nm ($R^2 = 0.72$). Another important region was seen in the visible blue centered on 428 nm across the SWIR1 (1000–1750 nm). The 75th percentile histogram showed that the visible blue wavelengths were the most frequent, followed by the NIR (around 733 nm), indicating that the visible blue wavelengths were correlated over a wider range of wavelengths than the highest correlated NIR wavelengths.

The MSVIs showed similar patterns to the HVIs (Fig. 5a–c). Overall, however, the correlation between MSVIs and ET was lower than for HVIs. The most highly correlated MSVI with ET involved MODIS band 3 (visible blue) and band 1(red), but with a ΔR^2 of −0.12 ($R^2 = 0.39$) compared to its HVI equivalent. MODIS band 4 (visible green) and band 1 were comparable to MODIS band 3 and band 1 ($R^2 = 0.37$). As with the HVIs, the MSVIs tended to be more highly correlated with the ET components, especially ET_S. Like the HVIs for ET_C, the top performing MSVI involved MODIS band 2 (VNIR) and band 1, but with a ΔR^2 of −0.17 ($R^2 = 0.51$). Similarly, the highest correlated MSVI for ET_S like the HVIs, involved MODIS band 6 (SWIR1) and MODIS band 3, but with a ΔR^2 of −0.14 ($R^2 = 0.58$). The MSVI involving MODIS band 5 (NIR) and MODIS band 3, like the HVIs, was nearly identical ($R^2 = 0.58$).

3.3. Ratio-based indices from the literature

The strength of the relationship between existing vegetation indices was low to moderate for ET and ET_S and moderate to high for ET_C (Table 5). In general, an MSBB structure-based index performed better than the water-based indices (NDWIs), while no single index category for HNBs was better across ET and its components. As in the exploratory analysis, HVIs performed better than their MSVI equivalents. Figs. 6 and 7 show the scatterplots of predicted ET

Table 5
Summary statistics of linear relationships of evapotranspiration (ET) or its components (c = canopy and s = soil) and 16 multi-spectral broadband and hyperspectral narrowband indices: coefficient of determination (R^2), statistical significance (p), intercept (b), slope with direction (m), and root mean squared error (RMSE). RMSE/μ is the relative RMSE or model RMSE divided by the observed mean (μ). The linear model with the highest R^2 and lowest RMSE is in bold for each category. The predicted values from models in bold versus observed LE are shown in Fig. 7. In each case, the number of samples was 26.

Index	ET							ET_C						ET_S					
	Abbreviation	R^2	p	b	m	RMSE (MJ m^2 d^{-1})	RMSE/μ (%)	R^2	p	b	m	RMSE (MJ m^2 d^{-1})	RMSE/μ (%)	R^2	p	b	m	RMSE (MJ m^2 d^{-1})	RMSE/μ (%)
Mutispectral broadband indices																			
Simple ratio	SR	0.10	0.123	10.33	0.12	4.00	33.94	0.26	0.008	6.49	0.21	3.77	41.99	0.05	0.289	3.83	−0.09	4.18	149.38
Normalized Difference Vegetation Index	NDVI	0.04	0.355	8.88	3.93	4.13	35.05	**0.51**	**<0.001**	**−2.37**	**15.37**	**3.08**	**34.32**	**0.29**	**0.004**	**11.25**	**−11.45**	**3.60**	**128.68**
Enhanced Vegetation Index	EVI	0.04	0.320	9.67	3.52	4.12	34.95	0.50	<0.001	1.29	12.81	3.08	34.34	0.28	0.006	8.38	−9.30	3.64	130.04
Visible Atmospherically Resistant Index	VARI	**0.37**	**<0.001**	**9.30**	**11.67**	**3.33**	**28.27**	0.42	<0.001	6.23	12.92	3.33	37.09	0.00	0.754	3.07	−1.26	4.28	152.68
Normalized Difference Water Index (1)	$NDWI_1$	0.29	0.005	9.14	25.65	3.55	30.14	0.02	0.533	8.32	6.38	4.34	48.38	0.16	0.046	0.82	19.26	3.94	140.57
Normalized Difference Water Index (2)	$NDWI_2$	0.17	0.038	7.41	11.74	3.84	32.56	0.19	0.026	4.15	12.99	3.94	43.92	0.00	0.835	3.27	−1.26	4.28	152.86
Normalized Difference Water Index (3)	$NDWI_3$	0.13	0.068	5.45	9.68	3.92	33.25	0.34	0.002	−1.51	16.04	3.57	39.76	0.06	0.248	6.97	−6.37	4.17	148.71
Hyperspectral narrowband indices																			
Hyperspectral Vegetation Index	HVI	0.15	0.051	9.48	0.34	3.88	32.91	0.44	<0.001	4.88	0.61	3.28	36.52	0.09	0.139	4.60	−0.27	4.09	146.05
Hypersepctral Normalized Difference Vegetation Index	HNDVI	0.11	0.092	6.33	7.30	3.96	33.60	**0.68**	**<0.001**	**−4.84**	**18.53**	**2.50**	**27.80**	0.26	0.008	11.18	−11.23	3.69	131.71
Greenness Index	GI	0.36	0.001	5.56	4.01	3.36	28.49	0.48	<0.001	1.56	4.78	3.17	35.32	0.01	0.580	4.00	−0.77	4.26	152.00
Hyperspectral Normalized Difference Water Index	HNDWI	0.36	0.001	9.36	25.85	3.35	28.48	0.03	0.415	8.28	7.45	4.32	48.10	0.18	0.032	1.08	18.40	3.89	138.78
Normalized Difference Infrared Index	NDII	0.24	0.011	6.88	13.72	3.66	31.06	0.27	0.006	3.56	15.16	3.73	41.59	0.00	0.805	3.32	−1.44	4.28	152.80
Water Index	WI	0.27	0.007	−11.09	20.24	3.60	30.53	0.01	0.645	13.33	−3.86	4.36	48.57	**0.37**	**0.001**	**−24.42**	**24.10**	**3.41**	**121.82**
Photochemical Reflectance Index	PRI	**0.40**	**<0.001**	**13.48**	**44.92**	**3.26**	**27.66**	0.34	0.002	10.62	43.24	3.55	39.59	0.00	0.911	2.86	1.66	4.28	152.96
Red-Edge Vegetation Stress Index	RVSI	0.10	0.124	10.16	52.44	4.00	33.94	0.50	<0.001	5.10	125.42	3.08	34.33	0.18	0.031	5.06	−73.02	3.88	138.65
Modified Chlorophyll Absorption Ratio Index	MCARI	0.15	0.048	9.16	11.65	3.87	32.86	0.40	<0.001	4.55	19.70	3.38	37.70	0.07	0.191	4.61	−8.05	4.13	147.53

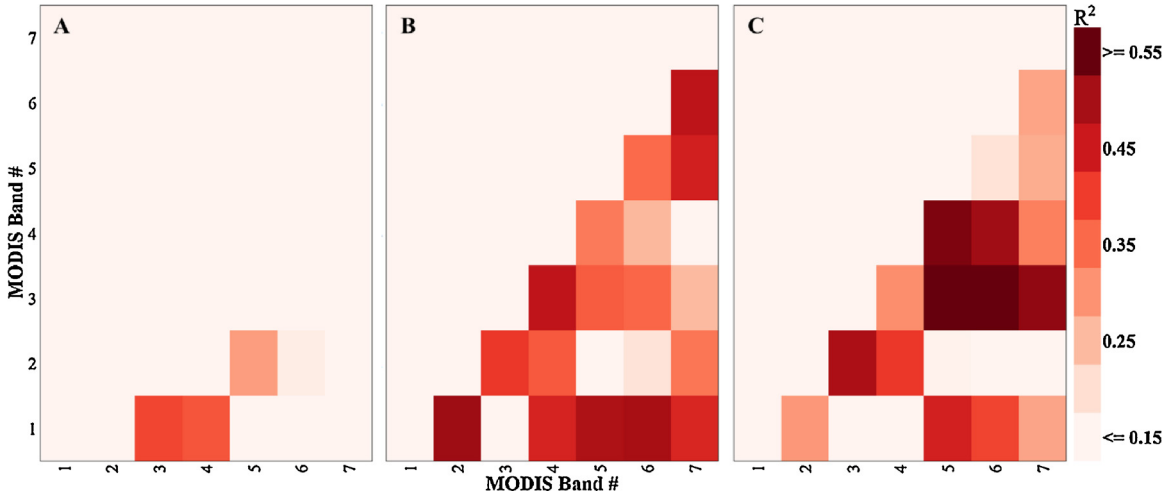

Fig. 5. Lambda–lambda contour plots showing the coefficient of determination (R^2) for every two-band multispectral broadband combination convolved to Moderate-Resolution Imaging Spectroradiometer (MODIS) spectral resolution for (a) evapotranspiration; (b) transpiration; and (c) soil evaporation.

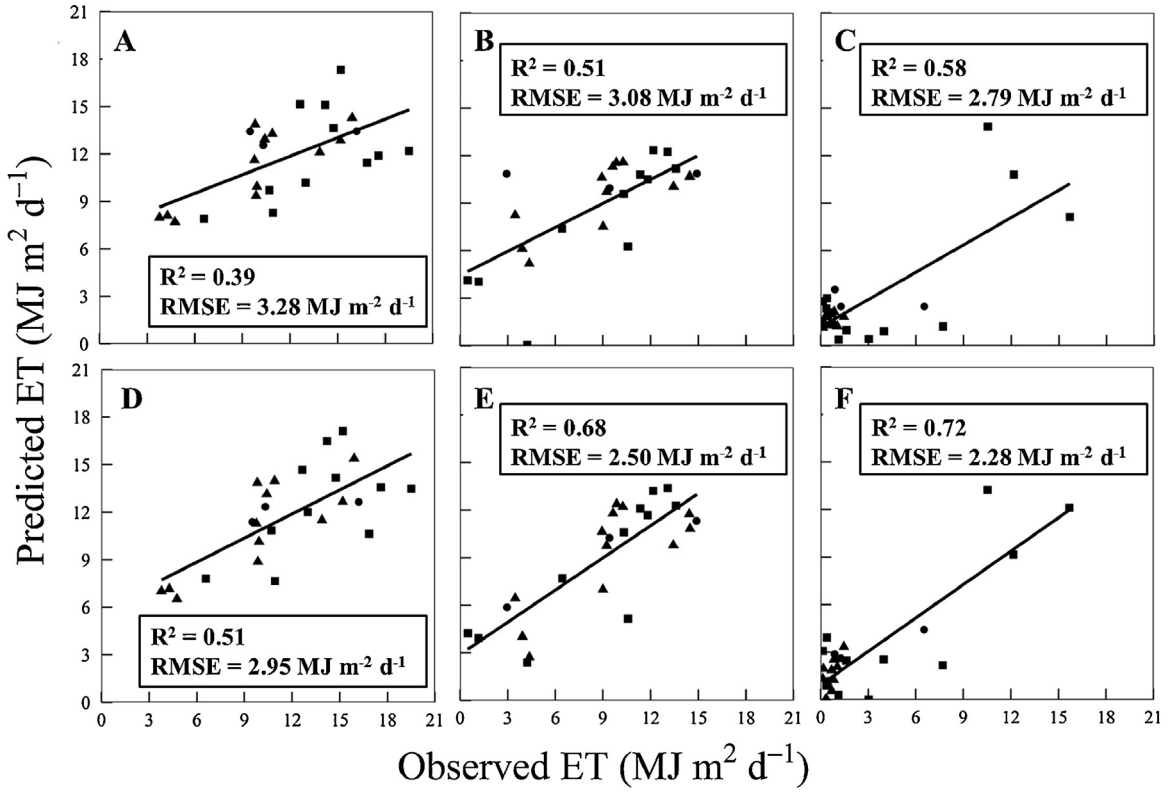

Fig. 6. Scatterplots of predicted evapotranspiration (ET) and its components (transpiration – ET_C and soil evaporation – ET_S) versus observed values for cotton (•), maize (▲), and rice (■). The upper panel (lower panel) shows the top performing multispectral broadband (hyperspectral narrowband) indices for each category from the exploratory analysis. The vegetation index for the models were MODIS band 3 and band 1 for ET (a); MODIS band 2 and band 1 for ET_C (b) and MODIS band 6 and band 3 for ET_S (c); 448 and 672 nm for ET (d), 672 and 733 nm for ET_C (e), and 743 and 953 nm for ET_S (f).

from the MSVIs and HVIs with the highest R^2 and lowest RMSE for the exploratory analysis and from the literature, respectively. In each case, higher R^2 corresponded to lower RMSE. For ET and ET_S, stronger relationships were observed in the exploratory analysis, while the optimal indices for ET_C identified in the exploratory analysis corresponded to indices in the literature. Although the correlations between indices from the literature and ET_C were higher than ET, the relative RMSE scores were also higher. For ET_S, the model RMSE exceeded mean observed ET_S by 100% for each index. For ET, VARI explained the most variance of the MSVIs (R^2 = 0.37, RMSE = 3.33 MJ/m^2/d, 28.27%), with a ΔR^2 of −0.04 compared to PRI, the best HVI for ET (R^2 = 0.40, RMSE = 3.26 MJ/m^2/d, 27.66%). For ET_C, the best performing MSVI was NDVI (R^2 = 0.51, RMSE = 3.08 MJ/m^2/d, 34.32%), with a ΔR^2 of −0.17 compared to its hyperspectral equivalent, HNDVI (R^2 = 0.68, RMSE = 2.50 MJ/m^2/d, 27.80%). The slope of the relationship between these indices and ET_C shown in Table 5 are both positive, meaning that as transpiration increased, NDVI and HNDVI increased. NDVI was the best MSBB predictor for ET_S as well (R^2 = 0.29, RMSE = 3.60 MJ/m^2/d, 128.68%), with a ΔR^2 of −0.08 compared to the Water Index derived from

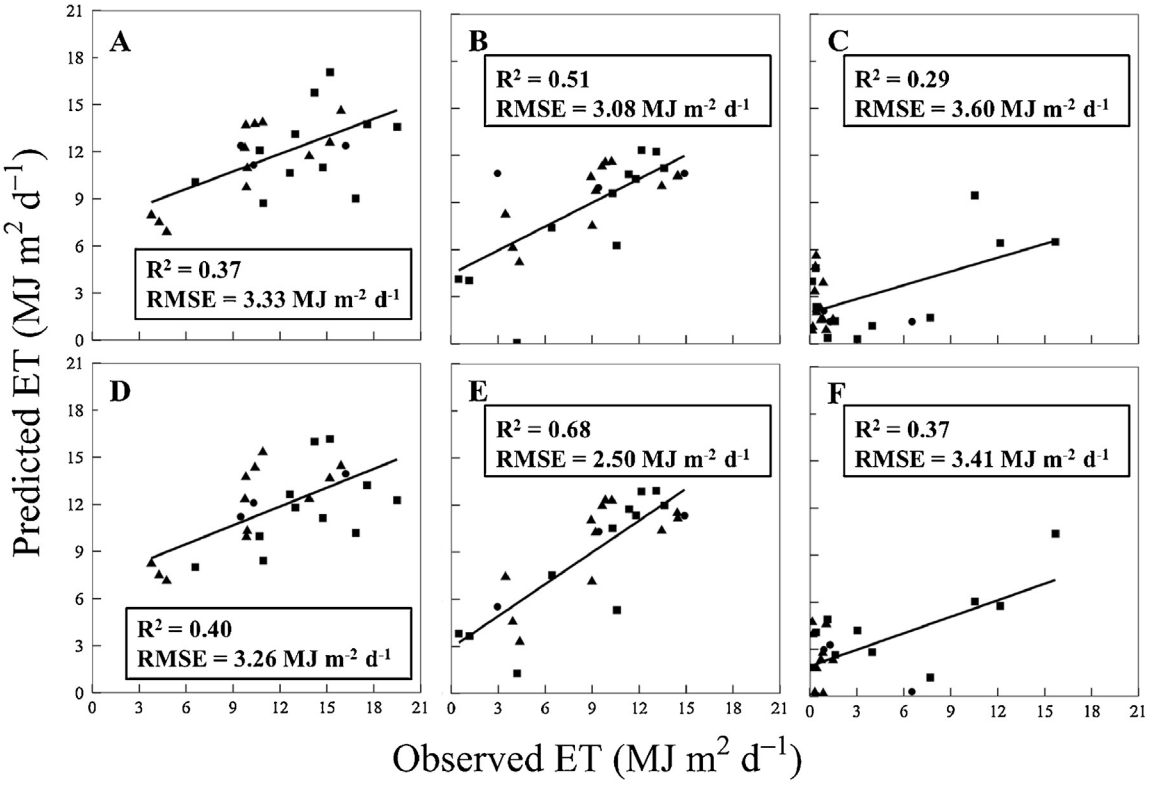

Fig. 7. Scatterplots of predicted evapotranspiration (ET) and its components (transpiration – ET_C and soil evaporation – ET_S) versus observed values for cotton (●), maize (▲), and rice (■). The upper panel (lower panel) shows the top performing multispectral broadband (hyperspectral narrowband) indices for each category. The predicted values are estimates from the linear models bolded in Table 5. The vegetation index for the models were the Visible Atmospherically Resistant Index for ET (a); Normalized Difference Vegetation Index for ET_C (b) and ET_S (c); Photochemical Reflectance Index for ET (d), Hyperspectral Normalized Difference Vegetation Index for ET_C (e), and Water Index for ET_S (f).

HNBs (R^2 = 0.37, RMSE = 3.41 MJ/m^2/d, 121.82%). The slope of the relationships from Table 5 are negative for NDVI and positive for WI, as expected, because in the former, as soil evaporation increased, transpiration decreased, and NDVI decreased, while in the latter, as transpiration decreased due to stress and wilting, soil evaporation increased and WI increased.

4. Discussion

This study evaluated the predictive ability of several HNBs and MSBBs to estimate ET and its components (transpiration and evaporation) for major water-intensive field crops in the Central Valley of California. The comparison was made between (1) ratio-based indices identified over the entire optical range available (428–2295 nm) at 10 nm intervals and (2) with ratio-based indices sensitive to plant biophysical/biochemical properties defined in the literature. The results make three important contributions to future Earth observation missions and the crop ET modeling community: (1) HVIs explained more ET variability than MSVIs in all cases; (2) transpiration was predicted well using indices in ET modeling (NDVI), while total ET was better predicted with other indices from the literature (PRI); and (3) soil evaporation was poorly predicted using indices from the literature, but the exploratory analysis revealed that NIR or visible blue and SWIR1 band combinations could possibly be used instead. The results correspond well with recent work that evaluated the relationship between long-term hyperspectral and CO_2 flux measurements taken from the rice fields on Twitchell Island using partial least squares regression (Matthes et al., 2015), but disagree to some extent with an analysis that compared hyperspectral indices over a smaller spectral range with CO_2 flux measurements taken in mountain grasslands (Balzarolo et al., 2015). As with other empirical studies, the robustness of the results of this study should be further scrutinized, because (1) the sample size was small and included only three field crops measured over the summer growing season for two years and (2) canopy absorption and scatter characteristics are often scale dependent. Potential studies could include using in situ and airborne/spaceborne remote sensing data in other ecosystems of the world, over different seasons, and for different crops, either empirically or by substituting vegetation indices used to drive process-based ET models with indices identified in this study.

4.1. Hyperspectral narrowbands (HNBs) versus multispectral broadbands (MSBBs) for total evapotranspiration (ET)

For ET, structure-based MSVIs performed considerably better than water-based MSBB indices, but worse than HVIs in general. VARI explained the most variability of the structure-based MSVIs, while Simp, NDVI, and EVI were the worst performers. Perry and Roberts (2008) observed that VARI performed better than other structure- and water-based indices for detecting crop water stress. Red-NIR indices (Simp, NDVI, and EVI) have been used to measure F_{IPAR}, F_{APAR}, and other biophysical properties, but are sensitive to canopy architecture, cell structure, leaf orientation (Gitelson et al., 2006), and saturate at high LAI due to the NIR component (Brantley et al., 2011). For these reasons, VARI may have performed better than the red-NIR indices, because it relies solely on visible light, which is less species-dependent, and scatter in the green due to chlorophyll that VARI detects, is much lower than scatter in NIR, which means the index saturates at much higher LAI than red-NIR indices. The performance of the water-based MSBB indices was more surprising, as they explained at least 21.6% less ET variance

than VARI, but are in theory more sensitive to plant physiology than structure-based indices. Perry and Roberts (2008) also observed that the water-based indices performed worse than VARI for detecting crop water stress, producing similar estimates for both stressed and non-stressed canopies, while Yebra et al. (2013) could not discern the superiority of any one structure-based or water-based index across crops. The water-based MSVIs are sensitive to leaf liquid water, which means the presence of soil background could be obscuring leaf water variability. The HNB water-based equivalents performed considerably better, meaning they may be less sensitive to mixed canopies. PRI, which uses HNBs in the visible range, yielded even higher predictive power than VARI. Unlike the red-NIR indices and VARI, PRI varies according to xanthophyll concentration, which changes when plants become stressed, and other accessory pigments at wavelengths indicative of light-use efficiency (Gamon et al., 1992). It therefore has been used extensively to measure the ET counterpart, CO_2 (see Peñuelas et al., 2011 for a review). Although the 672 nm HNB (maximum fluorescence) was used in many of the indices taken from the literature, the best performing indices from the exploratory analysis occurred by combining 672 with 448 nm (HNB) and MODIS band 3 and band 1 (MSBB), which explained 21.6% and 5.1% more ET variability than PRI and VARI, respectively. Leaf chlorophyll and accessory pigments (carotenoids and anthocyanin) all strongly absorb in the blue, however, the spectral region is not typically used for remote sensing, because of the strong absorption and scattering properties of the atmosphere.

4.2. Hyperspectral narrowbands (HNBs) versus multispectral broadbands (MSBBs) for transpiration (ET_C)

Existing MSVIs and HVIs predicted ET_C better than ET. The best MSVI and HVI for transpiration was NDVI. Transpiration is the dominant component of terrestrial ET (Schlesinger and Jasechko, 2014), which may explain why NDVI has been used so extensively and successfully in ET models. However, the hyperspectral equivalent explained 25% more variance in transpiration than the multispectral version and suffers less from saturation at high LAI (Oppelt and Mauser, 2004), revealing that modest improvements could be made by assimilating a hyperspectral equivalent of NDVI into ET models. As stated previously, NDVI is sensitive to the chlorophyll content of plants and therefore is used to measure biophysical properties such as F_{IPAR}. Since the partitioning method selected is a modeling approach taken from remote sensing and assumes F_{IPAR} drives ET_C, the ability of NDVI to predict ET_C may be inflated. Although no consistent pattern was observed between ET and F_{IPAR} across crop types or growth stages, field methods to partitioning, such as isotopic analysis, should be used to verify these results in the future. Since MSBB NDVI saturates for dense canopies as indicated by high LAI and the values for this study did not exceed seven, the relationship is likely to become non-linear in denser crop canopies. In this case, therefore, EVI, which performed comparably for transpiration and suffers less from saturation, should be used instead. PRI explained 50% less transpiration variance than HNDVI, which is unexpected, since it was the best performing index for ET and is used primarily to estimate light-use efficiency, which is an important control on ET_C. Light-use efficiency can vary significantly depending on environmental conditions, which affects the predictive ability of PRI, but no more than NDVI (Garbulsky et al., 2011). Perry and Roberts (2008) observed, however, that PRI was one of the worst performing indices for crop water stress and Thenot et al. (2002) noted that PRI was a good predictor only for well-watered canopies. The crops analyzed here were on a deficit schedule and therefore were likely stressed during grain/bud-filling.

4.3. Hyperspectral narrowbands (HNBs) versus multispectral broadbands (MSBBs) for soil evaporation (ET_S)

Although existing HVIs and MSVIs were relatively good predictors of ET_C, they were poor at predicting ET_S, especially later in the season when the canopy was closed. Ratio-based indices are designed primarily for the photosynthesizing portion of the canopy, so non-optical (microwave and thermal) remote sensing is often used to estimate soil moisture (see Wang and Qu, 2009 for a review). Two new combinations in the optical range should be explored for ET_S estimation. HVIs centered on two NIR bands (743 and 953 nm) explained 48.6% more ET_S variability than the best HVI taken from the literature (WI). Leaf water and soils both strongly scatter in the NIR, but leaf water absorbs strongly around 950–970 nm, while soils do not (Peñuelas et al., 1993). Perhaps the 953 nm and other nearby leaf water absorption bands act to standardize NIR scatter by the canopy and soil. The visible blue region stood out as a predictor for ET_S as well. The combination of HNB blue and SWIR1 bands (428 and 1518 nm $R^2 = 0.69$) and MODIS band 6 and band 3 explained 46.4 and 50.0% more ET_S variance than the best performing MSBB and HNB indices taken from the literature. Leaf water and soils absorb strongly in the blue, but leaf water absorbs strongly in the SWIR1 as well, especially around 1450 nm, while soils do not (Peñuelas et al., 1995). Perhaps the 1518 nm and other nearby leaf water absorption bands act to standardize blue absorption by the canopy and soil. Three rice samples at high ET_S clearly leverage the R^2 for ET_S, as demonstrated in the scatterplots and by the high relative RMSE. Unlike the other crops, which were infrequently wetted and only rarely during a field visit, rice was submerged in water. During the sprouting phase (when ET_S was high), the spectroradiometer was essentially measuring scatter from standing water with a very low vegetation signal. Given that the other crops and rice when the canopy was closed, had low ET_S relative to these leverage points, it may only be appropriate to use these indices for high ET_S.

5. Conclusion

This paper has demonstrated the strengths of hyperspectral narrowbands (HNBs) and hyperspectral ratio-based indices (HVIs) relative to multispectral broadbands (MSBBs) and MSBB ratio-based indices (MSVIs) in modeling crop evapotranspiration (ET) and its two primary components (transpiration and soil evaporation). In this paper, the most commonly used index (Normalized Difference Vegetation Index), explained half of the variability in transpiration, the largest component of ET. However, in the case of total ET and soil evaporation, other indices not commonly employed by the ET modeling community should be considered as substitutes. This could be done sufficiently in the case of total ET with existing HVIs, such as the Photochemical Reflectance Index, but not for soil evaporation. In the case of soil evaporation, two new ratio-based indices derived from NIR (743 and 953 nm) and visible blue (428 nm) and SWIR1 (1518 nm) show great promise and should be further studied. The combination of a hyperspectral NDVI and a newly identified hyperspectral soil index derived from hyperspectral remote sensing could, therefore, help to advance the understanding of micro- and macro-scale climate processes and forward agro-climatic information science, by reducing significant bias and error in an important component of existing ET models.

Acknowledgements

The project was funded primarily through support from the United States Geological Survey (USGS) Mendenhall Research

Fellowship Program under the direction of the Geographic Analysis and Monitoring and Land Remote Sensing programs. Field assistants (Tony Chang, Jeff Peters, and Bobbijean Freeman) who worked long and strenuous hours to collect spectroradiometric and ancillary biophysical data were funded with support from a USGS and National Association of Geoscience Teachers cooperative agreement. The micrometeorological stations were maintained through support from the California Energy Commission, USGS Federal Matching Funds program, U.S. Department of Energy's Office of Science Ameriflux program, California Department of Water Resources (CADWR), National Aeronautics and Space Administration (NASA), and the University of California (UC) at Berkeley and Davis. The authors are especially grateful to the following individuals, and their respective organizations, for outstanding contributions to the project: Diganta Adhikari, Christopher Lund, Forrest Melton, Dennis Baldocchi, Laura Koteen, Sara Knox, Cayle Little, and Richard Snyder for their assistance with deployment of field instrumentation, micrometeorological station ET data analysis and partial funding. We would also like to thank The Nature Conservancy for site access and logistical support for two of the micrometeorological stations. Finally, we would like to thank Deborah Soltesz, Miguel Velasco, Larry Gaffney, and Lois Hales who managed day-to-day logistics while personnel were in the field.

References

Allen, R.G., Pereira, L.S., Raes, D., Smith, M., 1998. Crop evapotranspiration – Guidelines for computing crop water requirements (No. 56). FAO – Food and Agriculture Organization of the United Nations, Rome, Italy.

Anderson, M.C., Norman, J.M., Diak, G.R., Kustas, W.P., Mecikalski, J.R., 1997. A two-source time-integrated model for estimating surface fluxes using thermal infrared remote sensing. Remote Sens. Environ. 60, 195–216.

Baldocchi, D.D., Hicks, B.B., Meyers, T.P., 1988. Measuring biosphere-atmosphere exchanges of biologically related gases with micrometeorological methods. Ecology 69, 1331–1340.

Balzarolo, M., Vescovo, L., Hammerle, A., Gianelle, D., Papale, D., Tomelleri, E., Wohlfahrt, G., 2015. On the relationship between ecosystem-scale hyperspectral reflectance and CO_2 exchange in European mountain grasslands. Biogeosciences 12, 3089–3108.

Biggs, T., Petropoulos, G.P., Velpuri, N.G., Marshall, M., Glenn, E.P., Nagler, P., Meβina, A., 2015. Remote sensing of Evapotranspiration from Cropland. In: Thenkabail, P.S. (Ed.), Remote Sensing Handbook (Volume III): Water Resources, Disasters, and Urban: Monitoring, Modeling, and Mapping. Taylor and Francis, London, United Kingdom, p. 673.

Blyth, E., Harding, R.J., 2011. Methods to separate observed global evapotranspiration into the interception, transpiration and soil surface evaporation components. Hydrol. Process. 25, 4063–4068.

Brantley, S.T., Zinnert, J.C., Young, D.R., 2011. Application of hyperspectral vegetation indices to detect variations in high leaf area index temperate shrub thicket canopies. Remote Sens. Environ. 115, 514–523.

Brunsell, N.A., Anderson, M.C., 2011. Characterizing the multi-scale spatial structure of remotely sensed evapotranspiration with information theory. Biogeosciences 8, 2269–2280.

CDFA, 2013. California Agricultural Statistics Review 2012–2013. California Department of Food and Agriculture, Sacramento, CA.

Chandrasekar, K., Sai, M.V.R.S., Roy, P.S., Dwevedi, R.S., 2010. Land Surface Water Index (LSWI) response to rainfall and NDVI using the MODIS Vegetation Index product. Int. J. Remote Sens. 31, 3987–4005.

Chapin, F.S., Matson, P.A., Vitousek, P., 2011. Principles of Terrestrial Ecosystem Ecology. Springer Science & Business Media.

Chen, D., Huang, J., Jackson, T.J., 2005. Vegetation water content estimation for corn and soybeans using spectral indices derived from MODIS near- and short-wave infrared bands. Remote Sens. Environ. 98 (October (2–3)), 225–236.

Courault, D., Seguin, B., Olioso, A., 2005. Review on estimation of evapotranspiration from remote sensing data: from empirical to numerical modeling approaches. Irrig. Drain. Syst. 19, 223–249.

Daly, C., Neilson, R.P., Phillips, D.L., 1994. A statistical-topographic model for mapping climatological precipitation over mountainous terrain. J. Appl. Meteorol. 33, 140–158.

Dam, J.C.V., Singh, R., Bessembinder, J.J.E., Leffelaar, P.A., Bastiaanssen, W.G.M., Jhorar, R.K., Kroes, J.G., Droogers, P., 2006. Assessing options to increase water productivity in irrigated river basins using remote sensing and modelling tools. Int. J. Water Resour. Dev. 22, 115–133.

Daughtry, C.S.T., Walthall, C.L., Kim, M.S., de Colstoun, E.B., McMurtrey III, J.E., 2000. Estimating corn leaf chlorophyll concentration from leaf and canopy reflectance. Remote Sens. Environ. 74, 229–239.

Decagon, 2010. AccuPAR PAR/LAI ceptometer model LP-80, Version 10. ed, Operator's Manual. Decagon Devices, Inc, Pullman, WA.

Diak, G.R., Mecikalski, J.R., Anderson, M.C., Norman, J.M., Kustas, W.P., Torn, R.D., DeWolf, R.L., 2004. Estimating land surface energy budgets from space: review and current efforts at the University of Wisconsin—Madison and USDA–ARS. Bull. Am. Meteorol. Soc. 85, 65–78.

Evans, R.G., Sadler, E.J., 2008. Methods and technologies to improve efficiency of water use. Water Resour. Res. 44, W00E04.

Falge, E., Reth, S., Brüggemann, N., Butterbach-Bahl, K., Goldberg, V., Oltchev, A., Schaaf, S., Spindler, G., Stiller, B., Queck, R., Köstner, B., Bernhofer, C., 2005. Comparison of surface energy exchange models with eddy flux data in forest and grassland ecosystems of Germany. Ecol. Model. 188, 174–216.

Fisher, J.B., Tu, K.P., Baldocchi, D.D., 2008. Global estimates of the land–atmosphere water flux based on monthly AVHRR and ISLSCP-II data, validated at 16 FLUXNET sites. Remote Sens. Environ. 112, 901–919.

Foken, T., 2008. The energy balance closure problem: an overview. Ecol. Appl. 18, 1351–1367.

Gamon, J.A., Peñuelas, J., Field, C.B., 1992. A narrow-waveband spectral index that tracks diurnal changes in photosynthetic efficiency. Remote Sens. Environ. 41, 35–44.

Gao, B., 1996. NDWI—A normalized difference water index for remote sensing of vegetation liquid water from space. Remote Sens. Environ. 58, 257–266.

Garbulsky, M.F., Peñuelas, J., Gamon, J., Inoue, Y., Filella, I., 2011. The photochemical reflectance index (PRI) and the remote sensing of leaf, canopy and ecosystem radiation use efficiencies: a review and meta-analysis. Remote Sens. Environ. 115, 281–297.

García-Mora, T.J., Mas, J.-F., Hinkley, E.A., 2012. Land cover mapping applications with MODIS: a literature review. Int. J. Digit. Earth 5, 63–87.

Gillies, R.R., Kustas, W.P., Humes, K.S., 1997. A verification of the "triangle" method for obtaining surface soil water content and energy fluxes from remote measurements of the Normalized Difference Vegetation Index (NDVI) and surface e. Int. J. Remote Sens. 18, 3145–3166.

Gitelson, A.A., Keydan, G.P., Merzlyak, M.N., 2006. Three-band model for noninvasive estimation of chlorophyll, carotenoids, and anthocyanin contents in higher plant leaves. Geophys. Res. Lett. 33, http://dx.doi.org/10.1029/2006GL026457.

Gitelson, A.A., Kaufman, Y.J., Stark, R., Rundquist, D., 2002. Novel algorithms for remote estimation of vegetation fraction. Remote Sens. Environ. 80, 76–87.

Gitelson, A.A., Merzlyak, M.N., Lichtenthaler, H.K., 1996. Detection of red edge position and chlorophyll content by reflectance measurements near 700 nm. J. Plant Physiol. 148, 501–508.

Glenn, E.P., Huete, A.R., Nagler, P.L., Hirschboeck, K.K., Brown, P., 2007. Integrating remote sensing and ground methods to estimate evapotranspiration. Crit. Rev. Plant Sci. 26, 139–168.

Glenn, E.P., Nagler, P.L., Huete, A.R., 2010. Vegetation index methods for estimating evapotranspiration by remote sensing. Surv. Geophys. 31, 531–555.

Gnyp, M.L., Miao, Y., Yuan, F., Ustin, S.L., Yu, K., Yao, Y., Huang, S., Bareth, G., 2014. Hyperspectral canopy sensing of paddy rice aboveground biomass at different growth stages. Field Crops Res. 155, 42–55.

Goetz, A.F.H., 2009. Three decades of hyperspectral remote sensing of the Earth: a personal view. Remote Sens. Environ. 113 (Suppl. 1), S5–S16 (Imaging Spectroscopy Special Issue).

Gowda, P.H., Chavez, J.L., Colaizzi, P.D., Evett, S.R., Howell, T.A., Tolk, J.A., 2008. ET mapping for agricultural water management: present status and challenges. Irrig. Sci. 26, 223–237.

Guerschman, J.P., Van Dijk, A.I.J.M., Mattersdorf, G., Beringer, J., Hutley, L.B., Leuning, R., Pipunic, R.C., Sherman, B.S., 2009. Scaling of potential evapotranspiration with MODIS data reproduces flux observations and catchment water balance observations across Australia. J. Hydrol. 369, 107–119.

Hardisky, M.A., Klemas, V., Smart, R.M., 1983. The influence of soil salinity, growth form, and leaf moisture on the spectral radiance of *Spartina alterniflora* canopies. Photogramm. Eng. Remote Sens. 49, 77–83.

Hatala, J.A., Detto, M., Sonnentag, O., Deverel, S.J., Verfaillie, J., Baldocchi, D.D., 2012. Greenhouse gas (CO_2, CH_4, H_2O) fluxes from drained and flooded agricultural peatlands in the Sacramento-San Joaquin Delta. Agric. Ecosyst. Environ. 150, 1–18.

Huete, A., 1988. A soil-adjusted vegetation index (SAVI). Remote Sens. Environ. 25, 295–309.

Huete, A., Didan, K., Miura, T., Rodriguez, E., Gao, X., Ferreira, L., 2002. Overview of the radiometric and biophysical performance of the MODIS vegetation indices. Remote Sens. Environ. 83, 195–213.

Huntington, T.G., 2006. Evidence for intensification of the global water cycle: review and synthesis. J. Hydrol. 319, 83–95.

Jung, M., Reichstein, M., Bondeau, A., 2009. Towards global empirical upscaling of FLUXNET eddy covariance observations: validation of a model tree ensemble approach using a biosphere model. Biogeosciences 6, 2001–2013.

Kalma, J.D., McVicar, T.R., McCabe, M.F., 2008. Estimating land surface evaporation: a review of methods using remotely sensed surface temperature data. Surv. Geophys. 29, 421–469.

Kang, M., Kwon, H., Cheon, J.H., Kim, J., 2012. On estimating wet canopy evaporation from deciduous and coniferous forests in the Asian monsoon climate. J. Hydrometeorol. 13, 950–965.

Katul, G.G., Oren, R., Manzoni, S., Higgins, C., Parlange, M.B., 2012. Evapotranspiration: a process driving mass transport and energy exchange in the soil–plant–atmosphere–climate system. Rev. Geophys. 50, RG3002.

Kool, D., Agam, N., Lazarovitch, N., Heitman, J.L., Sauer, T.J., Ben-Gal, A., 2014. A review of approaches for evapotranspiration partitioning. Agric. For. Meteorol. 184, 56–70.
Kustas, W.P., Norman, J.M., 1996. Use of remote sensing for evapotranspiration monitoring over land surfaces. Hydrol. Sci. J. 41, 495–516.
Leuning, R., Zhang, Y.Q., Rajaud, A., Cleugh, H., Tu, K., 2008. A simple surface conductance model to estimate regional evaporation using MODIS leaf area index and the Penman–Monteith equation. Water Resour. Res. 44, W10419.
Lu, X., Zhuang, Q., 2010. Evaluating evapotranspiration and water-use efficiency of terrestrial ecosystems in the conterminous United States using MODIS and AmeriFlux data. Remote Sens. Environ. 114, 1924–1939.
Marshall, M., Thenkabail, P., 2015. Developing in situ non-destructive estimates of crop biomass to address issues of scale. Remote Sens. 7, 808–835.
Matthes, J.H., Knox, S.H., Sturtevant, C., Sonnentag, O., Verfaillie, J., Baldocchi, D., 2015. Predicting landscape-scale CO_2 flux at a pasture and rice paddy with long-term hyperspectral canopy reflectance measurements. Biogeosci. Discuss 12, 5079–5122.
Merton, R., Huntington, J., 1999. Early simulation results of the ARIES-1 satellite sensor for multi-temporal vegetation research derived from AVIRIS. NASA Jet Propulsion Lab, Pasadena, CA.
Monteith, J., 1969. Light interception and radiative exchange in crop stands. Agron. Hortic. – Fac. Publ.
Moran, M.S., Clarke, T.R., Inoue, Y., Vidal, A., 1994. Estimating crop water deficit using the relation between surface-air temperature and spectral vegetation index. Remote Sens. Environ. 49, 246–263.
Mu, Q., Heinsch, F.A., Zhao, M., Running, S.W., 2007. Development of a global evapotranspiration algorithm based on MODIS and global meteorology data. Remote Sens. Environ. 111, 519–536.
Mu, Q., Zhao, M., Running, S.W., 2011. Improvements to a MODIS global terrestrial evapotranspiration algorithm. Remote Sens. Environ. 115, 1781–1800.
Nishida, K., Nemani, R.R., Running, S.W., Glassy, J.M., 2003. An operational remote sensing algorithm of land surface evaporation. J. Geophys. Res. Atmos. 108, http://dx.doi.org/10.1029/2002JD002062.
Norman, J.M., Kustas, W.P., Humes, K.S., 1995. Source approach for estimating soil and vegetation energy fluxes in observations of directional radiometric surface temperature. Agric. For. Meteorol. 77, 263–293 (Thermal Remote Sensing of the Energy and Water Balance over Vegetation).
Ollinger, S.V., 2011. Sources of variability in canopy reflectance and the convergent properties of plants. New Phytol. 189, 375–394.
Oppelt, N., Mauser, W., 2004. Hyperspectral monitoring of physiological parameters of wheat during a vegetation period using AVIS data. Int. J. Remote Sens. 25, 145–159.
Paw U, K.T.P., Qiu, J., Su, H.-B., Watanabe, T., Brunet, Y., 1995. Surface renewal analysis: a new method to obtain scalar fluxes. Agric. For. Meteorol. 74, 119–137.
Pearcy, R.W., Sims, D.A., 1994. Photosynthetic acclimation to changing light environments: scaling from the leaf to the whole plant. In: Exploitation of Environmental Heterogeneity by Plants: Ecophysiological Processes Above- and Belowground. Academic Press, San Diego, CA, pp. 145–174.
Pearson, R.L., Miller, L.D., 1972. Remote mapping of standing crop biomass for estimation of the productivity of the short-grass Prairie, Pawnee National Grassland, Colorado. In: 8th International Symposium on Remote Sensing of Environment, pp. 1357–1381.
Peñuelas, J., Garbulsky, M.F., Filella, I., 2011. Photochemical reflectance index (PRI) and remote sensing of plant CO_2 uptake. New Phytol. 191, 596–599.
Peñuelas, J., Baret, F., Filella, I., 1995. Semi-empirical indices to assess carotenoids/chlorophyll a ratio from leaf spectral reflectance. Photosynthetica 31, 221–230.
Peñuelas, J., Filella, I., Biel, C., Serrano, L., Save, R., 1993. The reflectance at the 950–970 nm region as an indicator of plant water status. Int. J. Remote Sens. 14, 1887–1905.
Penuelas, J., Pinol, J., Ogaya, R., Filella, I., 1997. Estimation of plant water concentration by the reflectance Water Index WI (R900/R970). Int. J. Remote Sens. 18 (13), 2869–2875.
Perry, E.M., Roberts, D.A., 2008. Sensitivity of narrow-band and broad-band indices for assessing nitrogen availability and water stress in an annual crop. Agron. J. 100, 1211.
Rodriguez, J.M., Ustin, S.L., Riaño, D., 2011. Contributions of imaging spectroscopy to improve estimates of evapotranspiration. Hydrol. Process. 25, 4069–4081.
Rosegrant, M.W., Ringler, C., Zhu, T., 2009. Water for agriculture: maintaining food security under growing scarcity. Annu. Rev. Environ. Resour. 34, 205–222.
Rouse, J.W., 1974. Monitoring the vernal advancement and retrogradation (green wave effect) of natural vegetation. Final rep. NASA/GSFC, Greenbelt, MD.
Schlesinger, W.H., Jasechko, S., 2014. Transpiration in the global water cycle. Agric. For. Meteorol. 189–190, 115–117.
Schuepp, P.H., Leclerc, M.Y., MacPherson, J.I., Desjardins, R.L., 1990. Footprint prediction of scalar fluxes from analytical solutions of the diffusion equation. Bound. Layer Meteorol. 50, 355–373.
Senay, G.B., Budde, M., Verdin, J.P., Melesse, A.M., 2007. A coupled remote sensing and simplified surface energy balance approach to estimate actual evapotranspiration from irrigated fields. Sensors 7, 979–1000.
Thenkabail, P.S., Smith, R.B., De Pauw, E., 2000. Hyperspectral vegetation indices and their relationships with agricultural crop characteristics. Remote Sens. Environ. 71, 158–182.
Thenkabail, P.S., Mariotto, I., Gumma, M.K., Middleton, E.M., Landis, D.R., Huemmrich, K.F., 2013. Selection of hyperspectral narrowbands (HNBs) and composition of hyperspectral twoband vegetation indices (HVIs) for biophysical characterization and discrimination of crop types using field reflectance and hyperion/EO-1 data. IEEE J. Sel. Top. Appl. Earth Observ. Remote Sens. 6, 427–439.
Thenot, F., Méthy, M., Winkel, T., 2002. The Photochemical Reflectance Index (PRI) as a water-stress index. Int. J. Remote Sens. 23, 5135–5139.
Thorne, J.H., Boynton, R., Flint, L., N'goc Le, T., 2012. Development and application of downscaled hydroclimatic predictor variables for use in climate vulnerability and assessment studies. University of California at Davis, Davis, CA.
Thorp, K.R., Tian, L., Yao, H., Tang, L., 2004. Narrow-band and derivative-based vegetation indices for hyperspectral data. Trans. ASAE 47, 291–299.
Ustin, S.L., Roberts, D.A., Gamon, J.A., Asner, G.P., Green, R.O., 2004. Using imaging spectroscopy to study ecosystem processes and properties. Bioscience 54, 523–533.
Wang, K., Dickinson, R.E., 2012. A review of global terrestrial evapotranspiration: observation, modeling, climatology, and climatic variability. Rev. Geophys. 50, RG2005.
Wang, L., Good, S.P., Caylor, K.K., 2014. Global synthesis of vegetation control on evapotranspiration partitioning. Geophys. Res. Lett. 41, 2014GL061439.
Wang, L., Qu, J.J., 2009. Satellite remote sensing applications for surface soil moisture monitoring: a review. Front. Earth Sci. China 3, 237–247.
Wilson, K., Goldstein, A., Falge, E., Aubinet, M., Baldocchi, D., Berbigier, P., Bernhofer, C., Ceulemans, R., Dolman, H., Field, C., Grelle, A., Ibrom, A., Law, B.E., Kowalski, A., Meyers, T., Moncrieff, J., Monson, R., Oechel, W., Tenhunen, J., Valentini, R., Verma, S., 2002. Energy balance closure at FLUXNET sites. Agric. For. Meteorol. 113, 223–243.
Yebra, M., Van Dijk, A., Leuning, R., Huete, A., Guerschman, J.P., 2013. Evaluation of optical remote sensing to estimate actual evapotranspiration and canopy conductance. Remote Sens. Environ. 129, 250–261.
Zarco-Tejada, P.J., Berjón, A., López-Lozano, R., Miller, J.R., Martín, P., Cachorro, V., González, M.R., de Frutos, A., 2005. Assessing vineyard condition with hyperspectral indices: leaf and canopy reflectance simulation in a row-structured discontinuous canopy. Remote Sens. Environ. 99 (November (3)), 271–287.